Journal of Physics D: Applied Physics

PAPER

Mn_2CrGa-based Heusler alloys with low net moment and high spin polarization

To cite this article: Wenyong Zhang *et al* 2018 *J. Phys. D: Appl. Phys.* **51** 255001

View the article online for updates and enhancements.

Related content

- Structural and magnetic transitions in cubic Mn3Ga
  P Kharel, Y Huh, N Al-Aqtash et al.
- Quaternary Heusler compounds Co2xRhxMnZ (Z=Ga, Sn, Sb): crystal structure, electronic structure, and magnetic properties
  Vajiheh Alijani, Juergen Winterlik, Gerhard H Fecher et al.
- Effect of Co substitution on the magnetic and electron-transport properties of Mn2PtSn
  Y Huh, P Kharel, A Nelson et al.

J. Phys. D: Appl. Phys. **51** (2018) 255001 (10pp) https://doi.org/10.1088/1361-6463/aac346

Mn_2CrGa-based Heusler alloys with low net moment and high spin polarization

Wenyong Zhang[1,2], Yunlong Jin[1,2], Ralph Skomski[1,2], Parashu Kharel[1,3], Xingzhong Li[1], Tingyong Chen[4], Gejian Zhao[4], Dongrin Kim[4], Shah Valloppilly[1] and David J Sellmyer[1,2]

[1] Nebraska Center for Materials and Nanoscience, University of Nebraska, Lincoln, NE 68588, United States of America
[2] Department of Physics and Astronomy, University of Nebraska, Lincoln, NE 68588, United States of America
[3] Department of Physics, South Dakota State University, Brookings, SD 57007, United States of America
[4] Department of Physics, Arizona State University, Tempe, AZ 85287, United States of America

E-mail: wenyong.zhang@unl.edu and dsellmyer@unl.edu

Received 27 February 2018, revised 13 April 2018
Accepted for publication 9 May 2018
Published 29 May 2018

Abstract

Mn_2CrGa-based Heusler compounds combining small magnetization with high spin polarization, fabricated by Fe and Pt substitution for Cr, are investigated experimentally and discussed in terms of sublattice site occupancies. X-ray diffraction and electron diffraction indicate that the parent alloy and $Mn_2Cr_{0.6}Fe_{0.4}Ga$ are normal cubic Heusler alloys with substantial chemical disorder, whereas $Mn_2Cr_{0.6}Pt_{0.4}Ga$ crystallizes in the tetragonal $D0_{22}$ structure. Magnetization measurements indicate that the spin structure of the parent alloy is essentially ferrimagnetic, but alloying with Fe or Pt reduces the net magnetization per formula unit from 0.40 μ_B in the parent alloy to nearly zero in the Fe case. The Curie temperature, the magnetoresistance, and the Andreev-reflection transport-spin polarization are less affected by the substitutions, the last changing from 65% in Mn_2CrGa to 60% and 61% in the Fe- and Pt-substituted alloys, respectively. The properties of these alloys are favorable for spintronics applications.

Keywords: Heusler alloys, ferrimagnetism, magnetoresistance, spin electronics

(Some figures may appear in colour only in the online journal)

1. Introduction

Half-metallic ferrimagnets that combine small or zero net magnetic moments with high spin polarization at the Fermi level have recently attracted much attention [1–8]. The materials are scientifically interesting, due to their unique electronic, magnetic, and transport properties, and technologically important in the context of spin-valve, magnetic-tunnel-junction, spin-transfer torque, and next-generation spintronic devices. Ideally, they combine low magnetization, to reduce stray-field effects, with high magnetic anisotropy and a high Curie temperature. Many of the compounds in consideration are from the Heusler family of compounds.

The electronic structure and magnetic properties of Heusler compounds and alloys are critically dependent on structure and disorder. Therefore, it is important to summarize here various structures and atomic positions in these materials in order to motivate the present research and facilitate subsequent discussion. Figure 1 and table 1 together explain the structures and atomic positions of the ordered and disordered Heusler alloys considered in this paper. The meaning of the colors is Mn (red and pink), Cr, Fe, and/or Pt (all yellow), and Ga (blue). The site disorder leading to solid solution in B2 and A2 structures is represented by mixed color sectors of the corresponding elements.

For convenience, in figure 1 the origin of the unit cells has been chosen with Mn atoms located at (0, 0, 0) positions. In the general case of a quarternary Heusler alloy with $\mathcal{Y}$-structure, (XX′YZ, Hg_2CuTi-prototype, spacegroup F-43m) as shown in figure 1(a), the four different atoms XX′YZ are arranged

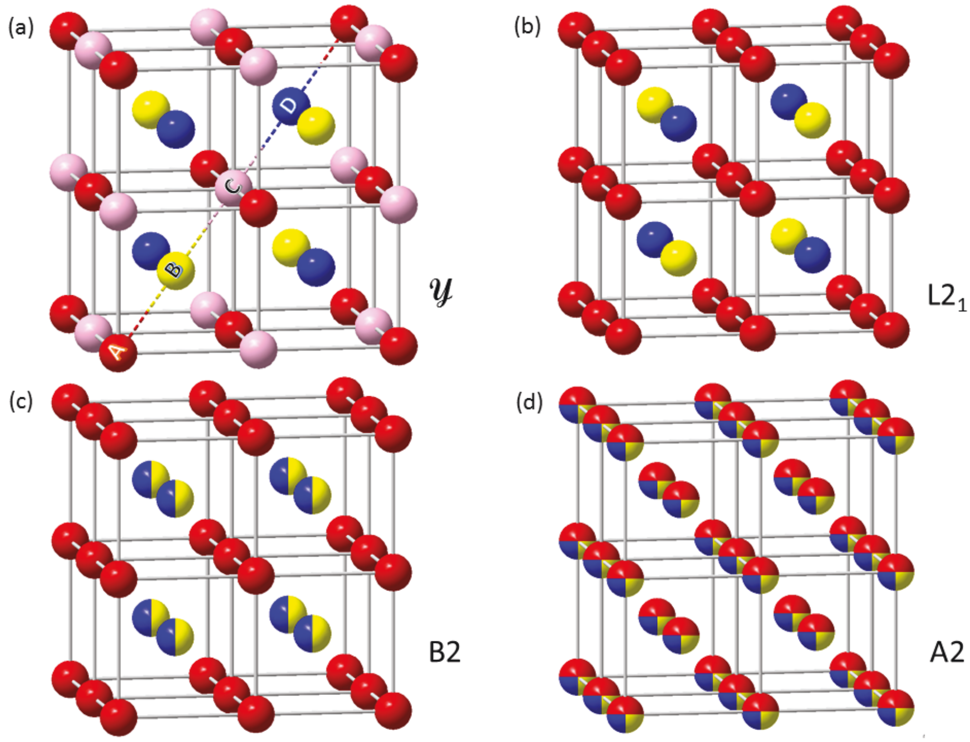

Figure 1. (a) Ordered quaternary $\mathcal{Y}$ structure (XX′YZ); (b) $L2_1$ ternary structure (X_2YZ); (c) partially disordered B2 structure (X_2YZ); and (d) fully disordered A2 structure (X_2YZ).

Table 1. Designation of Heusler structures.

Structure type of Heusler alloy	A	B	C	D
Quaternary Heusler (Y): (XX′)YZ	X	Y	X′	Z
Full Heusler ($L2_1$): X_2YZ	X	Y	X	Z
Half Heusler ($C1_b$): XYZ	X	Y		Z
Inverse Heusler (X_a): X2YZ	X	X	Y	Z
Partial disorder (B2): X_2YZ	X	Y/Z	X	Y/Z
Full disorder (A2): X_2YZ	X/Y/Z	X/Y/Z	X/Y/Z	X/Y/Z

along the cube diagonal on sites ABCD and they correspond to Wyckoff positions 4a, 4c, 4b and 4d, respectively. This structure is simplified to the $L2_1$-structure (X_2YZ, Cu_2MnAl-prototype, spacegroup *Fm*-3*m*) by choosing $X = X'$, as shown in figure 1(b), where the atoms are arranged ABAD along the cube diagonal. The corresponding Wyckoff positions are 4a and 4b for A atom sites, whereas sites B and D can be represented by Wyckoff positions 8c in *Fm*-3*m*. The $L2_1$ structure can be visualized as two interweaving sub-lattices of X and Y-Z atoms where both Y and Z atoms retain their specific atomic positions (B and D).The half-Heusler compound XYZ ($C1_b$ structure) is obtained from the Y structure by leaving the C atom site vacant. When there is some degree of intra-sublattice disorder between B and D sites of the $L2_1$ structure, the resultant will be a primitive lattice that can be represented by one half of the unit cell dimensions of the $L2_1$ structure and one eighth of its volume as in a CsCl-type (spacegroup Pm-3m) structure shown in figure 1(c). In this representation, the X atoms are located at the Wyckoff positions 1a and the Y and Z atoms are located at the Wyckoff positions 1b. Inter-sublattice disorder between X, Y and Z atoms lead to an A2-type (spacegroup Im-3m) bcc lattice with the same unit cell dimensions as the B2, as shown in figure 1(d). Here, all the atoms are represented by the Wyckoff positions 2a. The degree of chemical disorder greatly varies among Heuslers, depending on factors such as atomic size and chemical similarity, and it has become customary to use the term Heusler alloys in a rather broad sense, including substantial chemical disorder [9].

Tetragonal Heusler alloys are obtained by expanding or contracting the unit cell in the *c*-direction. The distortion is only partially understood [4], but it probably involves a quantum-mechanical admixture of Mn^{3+} character, $3d^4$ being a strong Jahn–Teller ion. The tetragonal alloys are normally described in terms of a different unit cell, characterized by a 45° rotation in the *a*-*b*-plane and $a \rightarrow a/\sqrt{2}$. Each of the structures in figure 1 has its own tetragonal equivalent. The $D0_{22}$ structure occurs in two variants, having $c/a \approx \sqrt{2}$ and

$c/a \approx 2$, and both variants are typically separated by an energy barrier [4]. The transition between the two variants is of the Bain type [10], where $c/a = \sqrt{2}$ and $c/a = 2$ correspond the underlying bcc and fcc lattices, respectively. This is important for the understanding of the x-ray diffraction (XRD) patterns of the Pt-substituted alloys (shown in figure 2).

The electronic structure of the Heuslers is intriguing because of its strong influence on magnetic properties. The full Heusler compound X_2YZ corresponds to X = Mn, Y = (Cr, Fe, Pt), and Z = Ga in the present study. The atomic positions are those of a $2 \times 2 \times 2$ supercell created from body-centered-cubic (bcc) unit cells, the X atoms occupying the corners and the Y and Z atoms in the central positions. This topology has far-reaching consequences for the electronic structures of the alloys. For example, in Mn_2YZ, the Mn–Mn exchange is limited to next-nearest or more distant neighbors and ferromagnetic.

Putting X = Y in the $L2_1$ structure (figure 1, table 1) yields the $D0_3$ (prototype Fe_3Al). One example is cubic Mn_3Ga, characterized by the Wyckhoff occupancies Mn 8c, Mn 4b, and Ga 4a. This means that Mn occupies two nonidentical sites, having different numbers of Mn nearest and next nearest neighbors. The $L2_1$, $D0_3$ and B2 structures all support a band gap and—subject to secondary spin splitting—half-metallicity, so long as the central atoms are sufficiently different from the corner atoms. Putting X = Y = Z, yields the bcc structure, whose electronic density of states is gapless.

The inverse cubic Heusler structure (X_a structure) of table 1 has the prototype Hg_2CuTi and differs from the normal cubic Heusler structure by half the X atoms interchanging positions with the Y or Z atoms. There is no longer a simple cubic sublattice exclusively occupied by X atoms, and the electronic structure of inverse cubic Heusler alloys is very different from that of normal cubic Heusler alloys. The X_a structure also supports half-metallicity, but based on a different mechanism, involving strong nearest-neighbor Mn–Mn interactions [11]. The stability of the X_a structure relative to the $L2_1$ structure may be an atomic-size effect (*d*-band contraction), the X_a order being favorable for small Y atoms. Mn_2CoZ and Mn_2NiZ tend to crystallize in the inverse structure [11], which has prompted us to focus on Fe and Pt substitutions. Note that both the normal and the inverse cubic Heusler structures are special cases of the quaternary Heusler structure ($\mathcal{Y}$ structure, prototype LiMgPdSn), which has the composition XX′YZ [10, 12].

Among the Heusler compounds, Mn-based alloys are of particular interest because they tend to have low moments and high Curie temperatures T_c and because some of them are predicted to be tetragonal, with the prospect of high magnetic anisotropy [13–15]. Much of the published literature on Mn_2YZ alloys with small net magnetization is theoretical in nature, using both first-principle calculations [3, 4, 16–18] and finite-temperature simulations [19, 20]. The range of experimental systems is limited so far, mainly because the structures assumed in the theoretical calculations do not form easily. In fact, Mn_2CoZ [11] and Mn_2CrGa [21] have been found to crystallize in the inverse cubic Heusler (X_a) and disordered CsCl (B2) structures, respectively. While chemical disorder is generally detrimental to the spin polarization at the Fermi level, the half-metallic character of Heusler alloys is often robust with respect to B2-type disorder [22–25]. A tetragonal distortion is also likely to yield a moderate reduction in spin polarization at the Fermi level [4]. The Heusler compounds Mn_2TGa (*T* = Mn, Fe, and Pt) also have been studied experimentally [26–31]. For *T* = Mn or Fe, up to the annealing temperature, the compound may be disordered cubic, $D0_{22}$ tetragonal, or $D0_{19}$ hexagonal structure [14, 32, 33]. In the $D0_{22}$ tetragonal *T* = Mn film, site occupancies are Ga on the 2a and Mn on 2b and 4d. The Mn on the 2b site has the larger moment of 3.07 μ_B. Its uniaxial anisotropy constant and saturation magnetization per formula unit (f.u.) are 1.0 MJ m^{-3} and 0.65–1.29 μ_B/f.u. [30]. In the $D0_{22}$ tetragonal *T* = Fe film, Ga and Mn atoms occupy both 2a and 2b sites; Fe shares the 4d site with Mn. Its uniaxial anisotropy constant and saturation magnetization are >1.0 MJ m^{-3} and about 1.5 μ_B/f.u. [31, 32]. It was reported that for *T* = Pt, the structure is the inverse tetragonal with the Curie temperature of 230 K [34]; Ga takes the 2a site, Mn occupies the 2b and 2c sites, and Pt is on the 2d site. The moments on the 2b and 2c sites are 3.65 μ_B and -3.1 μ_B. The 2b Mn antiferromagnetically aligns with the 2c Mn, leading to a net moment of 0.55 μ_B/f.u.

The $N_v - 24$ Slater–Pauling rule [3, 35], which describes full Heusler alloys, can be used to explore the concept of compensation in ferromagnetic Heusler compounds and alloys. For example, the simpler stoichiometry Mn_3Ga compound has $N_v = 24$ and a moment per formula unit of $m = 0$, but experiment shows that the alloy crystallizes in another structure [14], whereas $L2_1$-ordered ($D0_3$-ordered) bulk Mn_3Ga has remained hypothetical. So far, some potentially compensated Heusler ferrimagnets ($D0_{22}$ Mn_3Ge, $D0_3$ Mn_3Al, inverse tetragonal $Mn_{3-x}Pt_xGa$, cubic Mn_2Ru_xGa, $D0_{22}$ Mn_2Fe_xGa, $L2_1$ $(Mn_{1-x}Co_x)_2VGa$, and Hg_2CuTi-type Ti_2MnAl) have been synthesized [26, 31, 36–40]. The compensation is incomplete for most Heusler compounds. Half-Heusler Mn_2Ru_xGa has the Cl_b structure [38]; Mn, Ru, and Ga occupy the 4b, 4c, 4d, and 4a sites, respectively. Mn_2Ga is ferrimagnetic with $M_s = 1.65$ μ_B/f.u. and $T_c = 225$ K. Due to electron doping, $Mn_2Ru_{0.48}Ga$ is nearly fully compensated with $M_s = 0.1$ μ_B/f.u., $T_c = 460$ K, and 54% spin polarization [38]. Mn_2FeGa and Mn_2PtGa have been predicted to exhibit a tetragonally distorted ground state [4], which would support a lowest-order (second-order) magnetic anisotropy constant. Research on Mn_2YGa materials therefore offers four potentially very favorable properties, namely high spin polarization at the Fermi level, Curie temperature much above room temperature, low magnetization, and substantial anisotropy.

The focus of this paper is on transition-metal substitutions in Mn_2CrGa. The parent alloy has been predicted to be a half metal with T_c well above room temperature, to have a spin polarization of 76% in the completely ordered cubic $L2_1$ structure, and to exhibit a large magnetocrystalline anisotropy of about 2.46 MJ m^{-3} and a Curie temperature of 970 K in the tetragonal structure [16, 17]. The Mn moment (1.94 μ_B) is anti-parallel to Cr moment (-2.86 μ_B). Mn_2CrGa has $N_v = 23$ valence electrons per formula unit, namely seven per Mn atom, six per Cr atom, and three per Ga atom. The $N_v - 24$

Slater–Pauling rule therefore predicts a moment per formula unit m of magnitude 1 μ_B. Based on this, partial substitution of Fe (eight valence electrons) or Pt (ten valence electrons) for Cr (six valence electrons) could yield $N_v = 24$ and $m = 0$. We investigate this phenomenon in the present paper through a study of Mn_2CrGa, $Mn_2Cr_{1-x}Fe_xGa$ (x = 0–0.5), and $Mn_2Cr_{1-y}Pt_yGa$ (y = 0–0.4) produced by arc melting, rapid quenching, and annealing. X-ray diffraction, point-contact Andreev reflection (PCAR), and high-field magnetization measurements are used to characterize the alloys.

Aside from the magnetic moment, our focus is on structural aspects, such as the degree of Heusler order and a possible tetragonal distortion of the lattice, the spin polarization at the Fermi level, and the Curie temperature and anisotropy of the alloys. In this paper section 2 describes the experimental methods, section 3 presents and discusses our experimental results, and section 4 summarizes the research.

2. Experimental methods

Bulk Mn_2CrGa, $Mn_2Cr_{1-x}Fe_xGa$ (x = 0–0.5), and $Mn_2Cr_{1-y}Pt_yGa$ (y = 0–0.4) samples in the form of ribbons were prepared by arc melting, rapid quenching and annealing. First, the ingots were prepared by arc melting high-purity (99.95%) constituent elements in an argon atmosphere. In order to compensate for Mn loss, an extra 3% Mn by weight was added during arc melting. The crystalline ribbon samples were obtained by rapidly quenching the induction-melted materials onto the surface of a copper wheel rotating at 20 m s^{-1} in the melt-spinner chamber. These ribbons are about 2 mm wide and 50 μm thick. In order to obtain the equilibrium crystal structure, the ribbon samples were annealed at 500 °C for 2 h in a tubular furnace pumped to a base pressure of about 10^{-7} Torr. The crystal structure and phase components of the samples were investigated with x-ray diffraction and by analyzing the electron-diffraction patterns and element mapping data collected using a FEI Tecnai Osiris transmission electron microscope (TEM). The magnetic properties including field and temperature dependence of magnetization, and the electron-transport properties were measured using a Quantum Design physical property measurement system (PPMS) having a vibrating-sample-magnetometer option. The degree of transport-spin polarization was measured by PCAR [22, 41], recording the conductance spectra at the interface between the sample and a superconducting Pb tip at 1.8 K [41, 42].

3. Results and discussion

Figures 2(a)–(c) shows the Cu K_α XRD patterns of the Mn_2CrGa, $Mn_2Cr_{0.6}Fe_{0.4}Ga$, and $Mn_2Cr_{0.6}Pt_{0.4}Ga$ ribbons. The diffraction peaks of Mn_2CrGa and $Mn_2Cr_{0.6}Fe_{0.4}Ga$ were indexed to the cubic unit cell of the B2 structure, whereas for $Mn_2Cr_{0.6}Pt_{0.4}Ga$ the tetragonal unit cell of the $D0_{22}$ structure was used. The lattice parameter $a = 2.965$ Å of $Mn_2Cr_{0.6}Fe_{0.4}Ga$ is slightly smaller than that (2.969 Å) of Mn_2CrGa due to the smaller radius of the Fe atoms

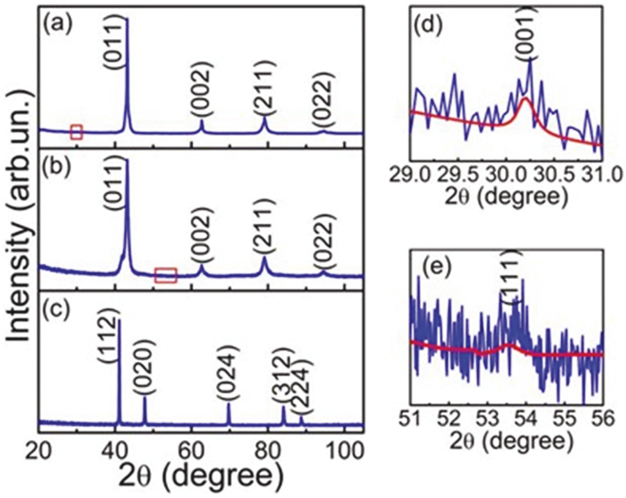

Figure 2. XRD patterns of the (a) Mn_2CrGa, (b) $Mn_2Cr_{0.6}Fe_{0.4}Ga$, (c) $Mn_2Cr_{0.6}Pt_{0.4}Ga$ samples. The red boxes in figures (a) and (b) are expanded in figures (d) and (e), respectively.

compared to Cr. The alloys are virtually single-phase. In particular, rhombohedral CrGa, which was previously found in $Mn_2Cr_{0.75}Pt_{0.25}Ga$ [21], has not been detected in the y = 0.4 sample. This indicates that further Pt addition suppresses the formation of CrGa. The c/a ratio of the tetragonal phase is very close to 2, meaning that the unit cell is essentially cubic and of the fcc type. The crystallographic identification of the tetragonal phase heavily relies on the peak intensities, which match the predictions for the $D0_{22}$ phase but are not consistent with a disordered fcc structure. The fractional site occupancies, as estimated from the model-based simulation of the $D0_{22}$ phase, are 90% Mn and 10% Pt on the 4d (0, ½, ¼) site; 60% Cr, 20% Pt and 20% Mn on the 2b (0, 0, ½) site; 100% Ga on the 2a (0, 0, 0) site.

The respective Mn_2CrGa and $Mn_2Cr_{0.6}Fe_{0.4}Ga$ samples exhibit a high degree of B2 order, as evidenced by figure 2, where (d) and (e) are expanded regions of (a) and (b). Note that the characteristic (0 0 1) and (1 1 1) B2 peaks are generally very small (section 1) and that the red curves in (d) and (e) assume an ordered B2 structure. Such weak, characteristic, diffraction peaks make it challenging to determine the site disorder from Rietveld analysis. Nevertheless, the B2 structural order parameter in these two samples can be roughly estimated by analyzing the intensities of (0 0 1) and (0 0 2) peaks as demonstrated by Bainsla *et al* [43]. By comparing the intensity ratio $I_{(0\,0\,1)}/I_{(0\,0\,2)}$ of both the experimental and simulated diffraction patterns, the order parameter S_{B2} was obtained to be 0.85 and 0.71 for Mn_2CrGa and $Mn_2Cr_{0.6}Fe_{0.4}Ga$ samples, respectively.

The TEM bright-field images, experimental electron diffraction patterns, and simulated electron-diffraction patterns of the three alloy samples are shown in figure 3. The bright-field images of the samples indicate that all samples contain micrometer-sized grains without any impurity phases. The electron-diffraction patterns of Mn_2CrGa (a) and $Mn_2Cr_{0.6}Fe_{0.4}Ga$ (b) are well reproduced by the patterns simulated for a B2-type cubic structure of Mn_2CrGa, indicating that there is no change in the crystal structure of Mn_2CrGa due to Fe substitution. The lattice parameter obtained from

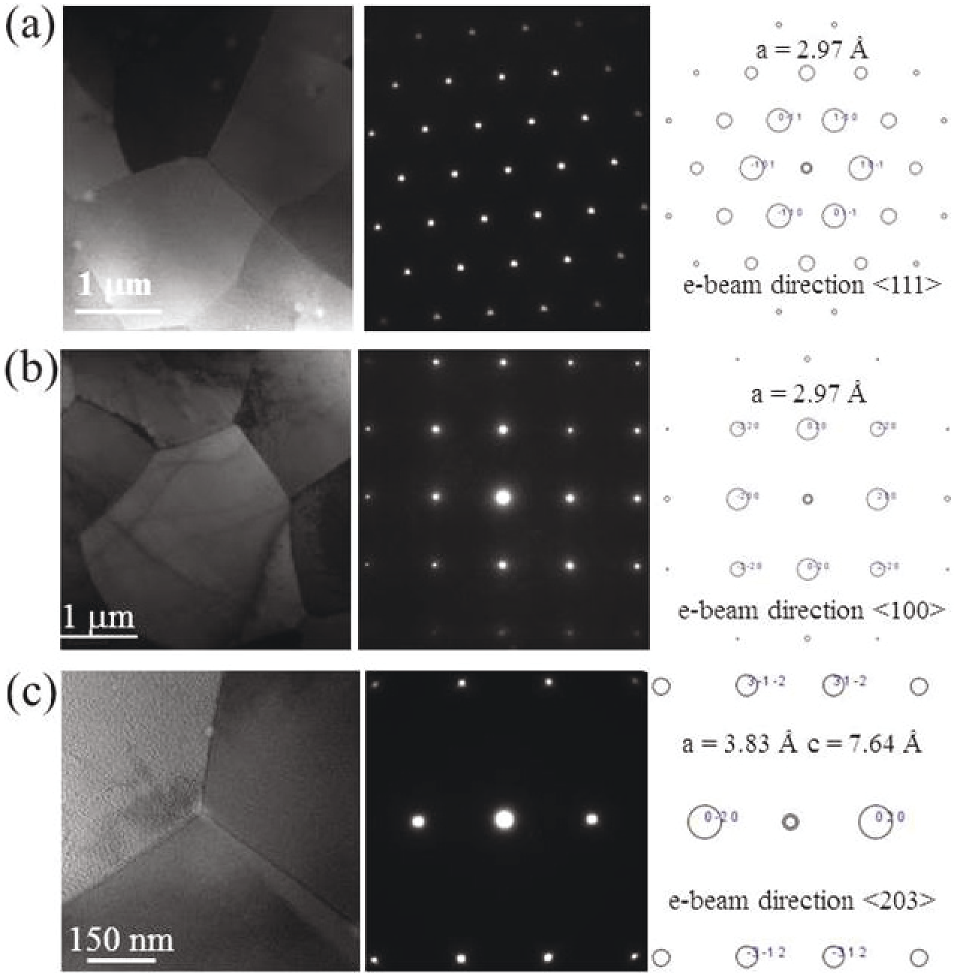

Figure 3. Bright-field TEM images, electron-diffraction spots, and simulated patterns of the ribbons: (a) Mn_2CrGa, (b) $Mn_2Cr_{0.6}Fe_{0.4}Ga$, and (c) $Mn_2Cr_{0.6}Pt_{0.4}Ga$.

the simulation is $a = 2.97$ Å for both samples. On the other hand, partial replacement of Cr by Pt yields a tetragonal ($D0_{22}$) crystal structure, with lattice parameters $a = 3.83$ Å and $c = 7.64$ Å, figure 1(c). These results agree well with the findings from the XRD analysis.

Figure 4(a) shows the temperature dependence of the magnetization $M(T)$. Mn_2CrGa has a high Curie temperature T_c of about 800 K, whereas the respective Curie temperatures of $Mn_2Cr_{0.6}Fe_{0.4}Ga$ and $Mn_2Cr_{0.6}Pt_{0.4}Ga$ are approximately 620 K and 570 K. A striking feature of all three samples is that the magnetization reaches a maximum below T_c. This feature is typical of ferrimagnets [44, 45] and implies the existence of two or more sublattices with different temperature dependences of the magnetization. For N magnetic sublattices, the intra- and intersublattice exchange constants J_{ij} form an $N \times N$ matrix whose diagonalization yields the mean-field Curie temperature. When N is very large, then the behavior tends to becomes spin-glass like. The number N reflects the atomic structure of the alloy. Perfectly $L2_1$-ordered Mn_2YGa has two magnetic sublattices associated with the 8c and 4b sites of Mn and Cr, respectively. The coupling between the Mn and Cr sublattices in Mn_2CrGa is antiferromagnetic, so that atomic moments of about 1 μ_B in both Mn and Cr [16] yield a ferrimagnetic net moment of 1 μ_B per formula unit. Chemical disorder creates new local environments, thereby enhancing the number N of magnetic sublattices. The effect is particularly pronounced for Mn, where the next-nearest-neighbor coupling, for example between the red atoms in figure 1(a), is ferromagnetic. However, nearest-neighbor Mn–Mn interactions are typically antiferromagnetic, so that site disorder involving Mn atom has a pronounced effect on the temperature dependence of the magnetization [34, 46, 47].

The results in [17] show that for Mn_2CrGa, the Mn sublattice carries a positive magnetic moment whereas the Cr sublattice has a negative moment. The substitution of Fe for Cr corresponding to electron doping favors the compensation of the magnetic moments from two sublattices. Therefore, $Mn_2Cr_{0.6}Fe_{0.4}Ga$ exhibits a completely compensated $M(T)$ curve similar to that observed in the Heusler compound $Mn_{1.5}FeV_{0.5}Al$ [48]. $x = 0.3$ and 0.5 samples exhibit under-compensated and overcompensated $M(T)$ curves shown in figure 4(b). $Mn_2Cr_{0.6}Pt_{0.4}Ga$ has a $D0_{22}$ structure. It was reported that $D0_{22}$-structure Mn_3Ga has two Mn sublattice sites (2b and 4d), and that the Mn moment on the 2b site is larger than that on the 4d site [30]. For the $Mn_2Cr_{0.6}Pt_{0.4}Ga$, Cr and Pt may replace the 2b-site Mn, favoring the cancelling of moments from two Mn sublattices and leading to a large reduction of net magnetization as shown in figure 4(a). The

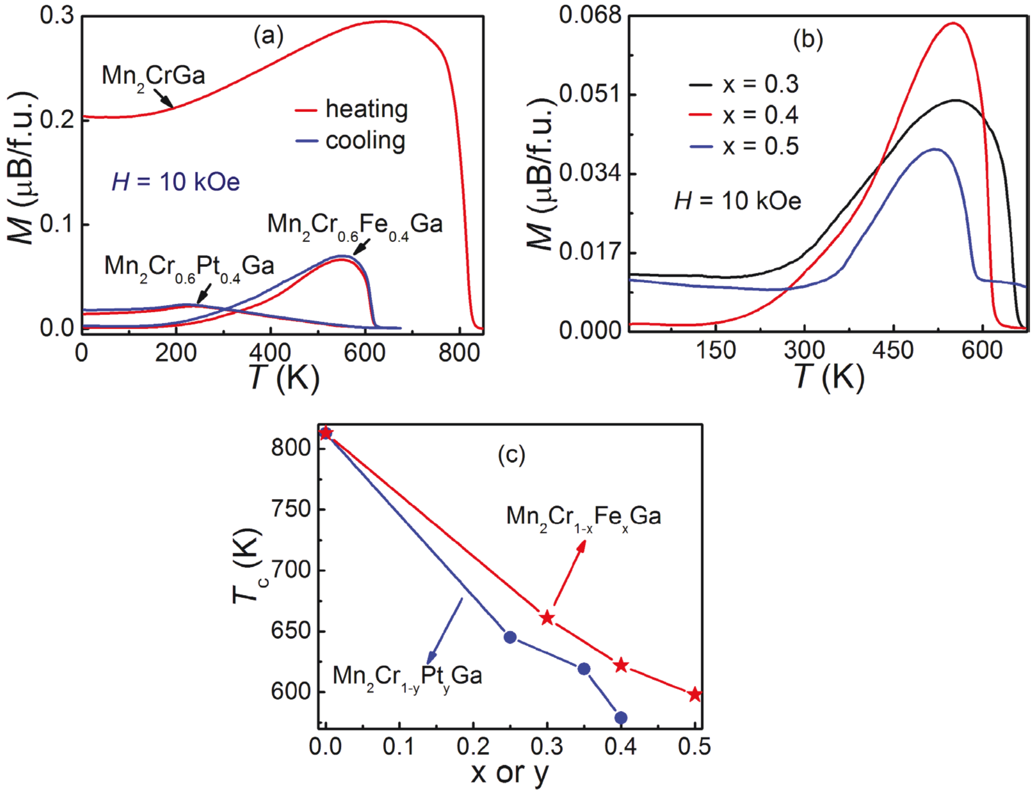

Figure 4. (a) Thermomagnetic curves of the Mn_2CrGa, $Mn_2Cr_{1-x}Fe_xGa$ (x = 0.4), and $Mn_2Cr_{1-y}Pt_yGa$ (y = 0.4), (b) $M(T)$ curves of the $Mn_2Cr_{1-x}Fe_xGa$ and (c) the Fe- or Pt-content dependence of the Curie temperature (T_c) for the $Mn_2Cr_{1-x}Fe_xGa$ and $Mn_2Cr_{1-y}Pt_yGa$.

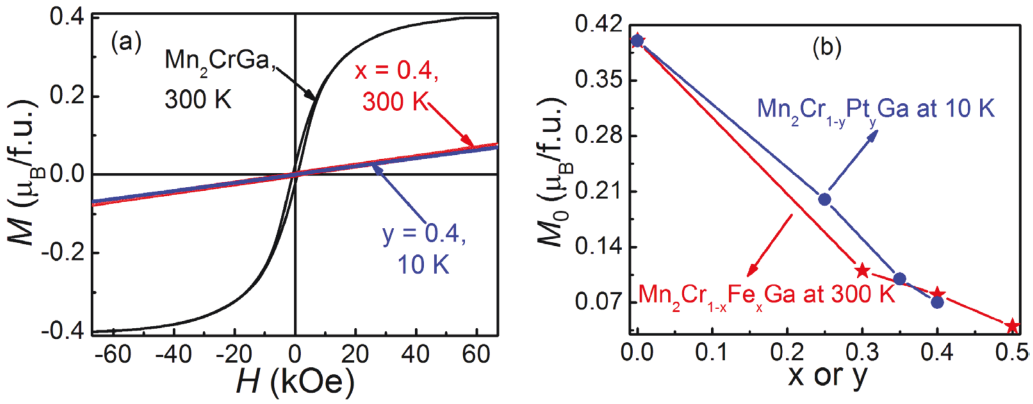

Figure 5. (a) $M(H)$ curves at 10 K or 300 K for the Mn_2CrGa, $Mn_2Cr_{0.6}Fe_{0.4}Ga$, and $Mn_2Cr_{0.6}Pt_{0.4}Ga$, (b) the Fe- or Pt-dependence of M_0 for the $Mn_2Cr_{1-x}Fe_xGa$ and $Mn_2Cr_{1-y}Pt_yGa$.

decrease of magnetization below 230 K is due to the compensation effect. Figure 4(c) shows the Fe- or Pt-content dependence of T_c for the $MnCr_{1-x}Fe_xGa$ and $Mn_2Cr_{1-y}Pt_yGa$. T_c presumably decreases with x or y due to the strengthening of the antiferromagnetic exchange interactions.

Figure 5(a) shows the magnetization as a function of the external magnetic field. Both the $M(T)$ curves of figure 4 and the $M(H)$ curves of figure 5 confirm that the Fe and Pt substitutions drastically reduce the magnetization. Since the anisotropy should be near zero as the ordering temperature is approached, we may use the maxima in figure 4 to estimate the net moment per formula unit from the respective 10 kOe magnetization. This yields approximately 0.3, 0.08 and 0.03 μ_B/f.u. for Mn_2CrGa, $Mn_2Cr_{0.6}Fe_{0.4}Ga$, and $Mn_2Cr_{0.6}Pt_{0.4}Ga$, respectively. Note that in figure 5(a), the saturation value of M for Mn_2CrGa is about 0.4 μ_B/f.u., and that the value of M at 65 kOe (M_0) for $Mn_2Cr_{0.6}Fe_{0.4}Ga$ at 300 K and for $Mn_2Cr_{0.6}Pt_{0.4}Ga$ is about 0.07 μ_B/f.u. It can be seen that all $M(H)$ curves in figure 5 exhibit high-field slopes of the order of 0.008 μ_B/kOe, which is typical for intersublattice exchange competing against Zeeman interactions. The relatively low value of 0.4 μ_B for Mn_2CrGa, compared to the theoretical value of 1 μ_B, may reflect chemical disorder and intersublattice non-collinearities. As in figure 4, the relative effect is the smallest for Mn_2CrGa. In the substituted alloys, it is amplified by the higher degree of disorder and by the lower net magnetization. Figure 5(b) shows the Fe- and Pt-content dependence of M_0 for the $MnCr_{1-x}Fe_xGa$ and $Mn_2Cr_{1-y}Pt_yGa$. M_0 decreases with x

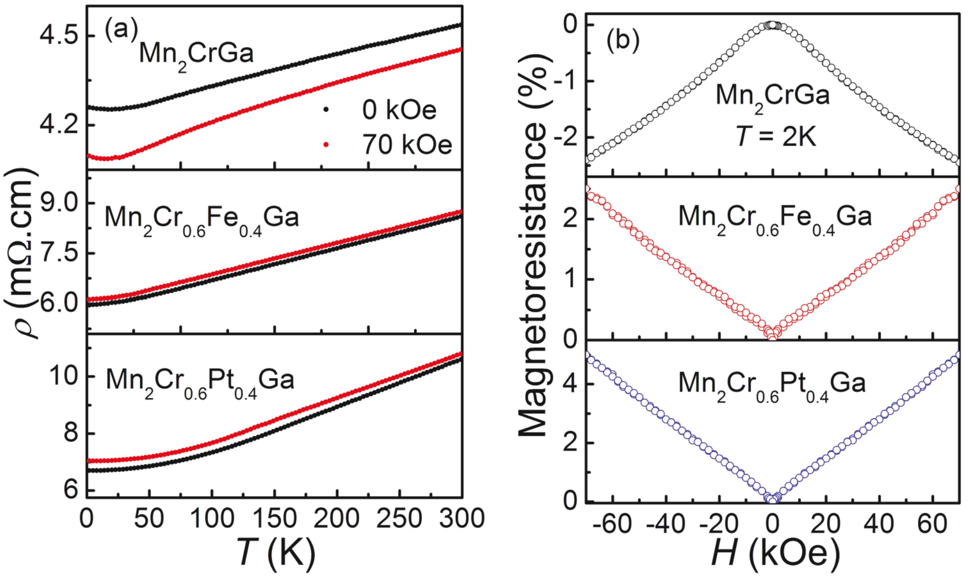

Figure 6. Transport behavior: (a) resistivity $\rho(T)$ in magnetic fields of 0 kOe and 70 kOe and (b) magnetoresistance $\Delta\rho(H)/\rho(0)$.

or y. The very low moment of cubic $Mn_2Cr_{0.6}Fe_{0.4}Ga$ is possibly due to the larger number of valence electrons compared to Mn_2CrGa. It is assumed that the substitution of Cr and Pt for 2b site Mn in $D0_{22}$ Mn_3Ga gives rise to a low net magnetization for the $Mn_2Cr_{0.6}Pt_{0.4}Ga$. The magnetic anisotropy constant K_1 of Mn_2CrGa is 0.18 MJ m^{-3} [1.8 Merg cm^{-3}], as determined by using the law-of-approach to saturation to fit the high-field part of $M(H)$ curve in figure 5. The magnetic anisotropies of $Mn_2Cr_{0.6}Fe_{0.4}Ga$ and $Mn_2Cr_{0.6}Pt_{0.4}Ga$ could not be extracted from the present experiment, because the anisotropy field $2K_1/M_0$ is very large due to the small net magnetization M_0.

The temperature-dependent resistivities $\rho(T)$ in fields of 0 kOe and 70 kOe and the magnetoresistance $[\rho(H) - \rho(0)]/\rho(0)$ are shown in figure 6. All samples exhibit a behavior reminiscent of bad or dirty metals [49–51], with huge residual resistivities in excess of 4000 $\mu\Omega$cm and a small or negative temperature coefficient at very low temperatures. The high residual resistivities probably reflect the B2-type chemical disorder, which primarily involves the chemically very different *Y* and Z atoms. The suppression of this effect remains a challenge to future research. As shown in figure 6(b), the magnetoresistance of the Mn_2CrGa sample is negative, whereas $Mn_2Cr_{0.6}Pt_{0.4}Ga$ and $Mn_2Cr_{0.6}Fe_{0.4}Ga$ exhibit positive magnetoresistances of 5.0% and 2.5%, respectively. Positive magnetoresistance is often observed in materials with antiferromagnetic couplings and some spin noncollinearity, because the external magnetic field makes the spins more parallel and reduces electron scattering due to misaligned spins. Since ρ at $H = 0$ and 70 kOe has been measured continuously from 2 K to 300 K and the black and the red curves do not cross at different temperature in figure 6(a), the MR of the three samples at different temperatures are very similar to figure 6(b) except that the magnitude varies slightly, as shown in figure 6(a).

The degree *P* of transport-spin polarization was measured using PCAR, recording the conductance spectra at the interface between the sample and a superconducting Pb tip at 1.8 K [41, 42]. In this technique, a current is injected from a normal metal into a singlet superconductor. For the electron to enter into the superconductor and proceed as a part of supercurrent, it must be paired with another electron of opposite spin leaving a hole in the interface which propagates away from the interface (Andreev reflection). In the case of a half metal with no minority spin states at the Fermi level, there is no Andreev reflection and thus the conductance across the half metal-superconductor interface is zero. Therefore, for magnetic materials, the Andreev reflection is limited by the minority spin states available at the Fermi level. In our experiment, the value of *P* was extracted by analyzing the PCAR spectra using the modified Blonder–Tinkham–Klapwijk (BTK) model in the ballistic and diffusive regime taking into account factors such as interfacial scattering ($\mathcal{Z}$), inelastic scattering, temperature, superconducting gap, and extra resistance [41, 42, 52, 53].

Some representative PCAR data from the samples Mn_2CrGa, $Mn_2Cr_{0.6}Pt_{0.4}Ga$, and $Mn_2Cr_{0.6}Fe_{0.4}Ga$ are shown in figure 7. The open circles are the experimental data and the solid curves are the best fits to the BTK model. During fitting, the temperature (T) and the superconducting gap (Δ) were set as experimental values while the spin polarization (P), $\mathcal{Z}$ and additional resistance (r_E) were varied. The effect of different parameters has been discussed before [54].

To physically interpret PCAR spectra, it is necessary to perform an extrapolation to $\mathcal{Z} = 0$ (clean interface). An example is the spin polarization of Mn_2CrGa alloys as a function of $\mathcal{Z}$, figure 7(d). The extrapolated transport spin polarizations are $64.2\% \pm 1.1\%$ for Mn_2CrGa, $60.6\% \pm 2.5\%$ $Mn_2Cr_{0.6}Pt_{0.4}Ga$, and $59.8\% \pm 0.8\%$ for $Mn_2Cr_{0.6}Fe_{0.4}Ga$. It is difficult to draw conclusions from these numbers because the extrapolated *P* values tend to be smaller than the actual spin polarizations in the materials; as a rule of thumb, *P* values significantly larger than 50% are expected for materials approaching half-metallicity, whereas many magnetic metals have $P \approx 0$. Our measurements show that the substitution of Fe and Pt for Cr yields a substantial change in the magnetic

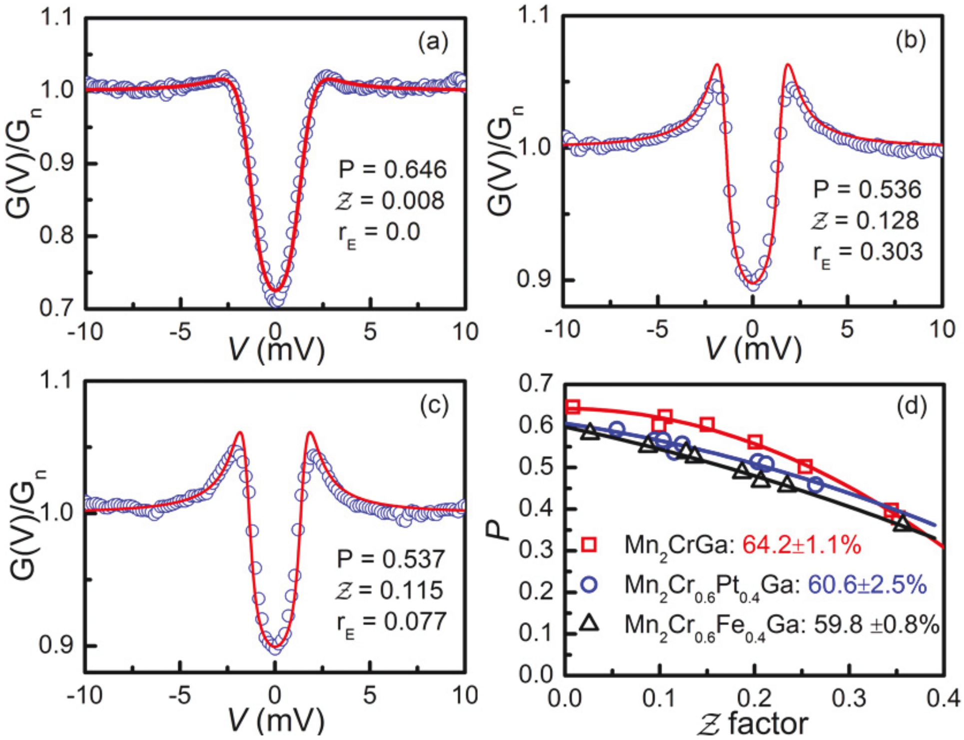

Figure 7. PCAR spectra (open circles) and BTK fit (solid curves) for (a) Mn_2CrGa, (b) $Mn_2Cr_{0.6}Fe_{0.4}Ga$, (c) $Mn_2Cr_{0.6}Pt_{0.4}Ga$, and (d) spin polarization of three samples as a function of the $\mathcal{Z}$-factor.

properties of Mn_2CrGa but leaves the spin polarization almost unchanged. Note that our spin polarizations are comparable to those measured in $L2_1$ ordered Co_2MnGe and Co_2MnSi, well ordered LiMgPdSn-type CoFeMnGe button ($P = 70\%$), and the B2-type disordered CoFeCrAl films [6, 55–57].

From the viewpoint of the relationship between atomic structure and electronic structure, the present findings about spin polarization have two aspects. First, for the reasons discussed in section 1, B2 disorder has a rather small effect on the half-metallicity. $Mn_2Cr_{0.6}Fe_{0.4}Ga$ contains substantial chemical disorder on the 4b sublattice in figure 1(c), but this disorder does not yield qualitative changes to band-gap formation so long as the Mn occupancy of the 8c sublattice is maintained. Second, $Mn_2Cr_{0.6}Pt_{0.4}Ga$ involves a more complicated scenario. Both the tetragonal distortion from $D0_3$ to $D0_{22}$ and the transition from the idealized $L2_1$ structure of figure 1(a) to the $D0_3$ structure of figure 1(b) may reduce the spin polarization [4]. However, the $D0_3$ structure differs from the $L2_1$ structure by partial site inversion, as contrasted to the A2 disorder (absence of B2 order), and site inversion tends to conserve half-metallicity in Mn_2YGa for Y atoms lighter than Ni [3]. The red atoms in figure 1(b) are now a mixture of Mn, Cr, and Pt atoms; that is, some Mn atoms may leave the 8c sublattice and occupy 4b sites. However, by itself, this mechanism does not negatively affect band-gap formation and half-metallicity so long as there are yellow atoms on the 4a (or even 4b) sites. Thus, the key structural feature of $L2_1$ half-metallicity is the distinction between transition-metal atoms on their regular 8c sites and different elements on the 4b and/or 4a sites. In general, all of the investigated Heusler alloys have similar and high values of spin polarization.

4. Conclusions

In summary, we have used Fe and Pt substitutions to reduce the net moment of the ferrimagnetic Heusler alloy Mn_2CrGa to nearly zero, without much change in the high transport spin polarization. By Pt substitution, we have succeeded in producing a tetragonal Heusler alloy while, at the same time, suppressing the formation of a secondary CrGa phase. The Curie temperatures of the substituted alloys are somewhat reduced due to additional antiferromagnetic exchange interactions but remain well above room temperature. The effect of the chemical disorder created by substitution is larger for Pt than for Fe, which we explain by the occupancy of the sublattices in the ternary Heusler alloys. Our results are important for the understanding and development of compensated ferrimagnets for spin-electronics applications.

Acknowlegments

Experimental work is supported by NSF-DMREF: SusChEM (1436385), and theoretical work by USDoE (DE-FG02-04ER46152). The research was performed in part in the Nebraska Nanoscale Facility: National Nanotechnology Coordinated Infrastructure and the Nebraska Center for Materials and Nanoscience, which are supported by the National Science Foundation under Award ECCS: 1542182, and the

Nebraska Research Initiative. Research at Arizona State is supported by DoE-SC0012670.

ORCID iDs

Wenyong Zhang https://orcid.org/0000-0002-8614-8318

References

[1] Jungwirth T, Marti X, Wadley P and Wunderlich J 2016 Antiferromagnetic spintronics *Nat. Nanotechnol.* **11** 231
[2] Park B G *et al* 2011 A spin-valve-like magnetoresistance of an antiferromagnet-based tunnel junction *Nat. Mater.* **10** 347
[3] Wollmann L, Chadov S, Kübler J and Felser C 2014 Magnetism in cubic manganese-rich Heusler compounds *Phys. Rev.* B **90** 214420
[4] Wollmann L, Chadov S, Kübler J and Felser C 2015 Magnetism in tetragonal manganese-rich Heusler compounds *Phys. Rev.* B **92** 064417
[5] Bainsla L and Suresh K G 2016 Equiatomic quaternary Heusler alloys: a material perspective for spintronic applications *Appl. Phys. Rev.* **3** 031101
[6] Graf T, Felser C and Parkin S S P 2011 Simple rules for the understanding of Heusler compounds *Prog. Solid. State Chem.* **39** 1
[7] Hu X 2012 Half-metallic antiferromagnet as a prospective materials for spintronics *Adv. Mater.* **24** 294
[8] Li J, Liu H, Zhang Z D, Zhang S L and Xu X W 2014 Obtaining half-metallic ferrimagnetism and antiferromagnetism by doping Mn and Fe for DO_3-type Heusler compound Cr_3Si *J. Alloy Compd.* **597** 8
[9] Sanvito S, Oses C, Xue J, Tiwari A, Zic M, Archer T, Tozman P, Venkatesan M, Coey J M D and Curtarolo S 2017 Accelerated discovery of new magnets in the Heusler alloy family *Sci. Adv.* **3** e1602241
[10] Bain E C 1924 The nature of martensite *Trans. Metall. Soc. AIME* **70** 25
[11] Liu G D, Dai X F, Liu H Y, Chen J L, Li Y X, Xiao G and Wu G H 2008 Mn_2CoZ (Z = Al, Ga, In, Si, Ge, Sn, Sb) compounds: structure, electronic, and magnetic properties *Phys. Rev.* B **77** 014424
[12] Choudhary R, Kharel P, Valloppilly S R, Jin Y L, O'Connell A, Huh Y, Gilbert S, Kashyap A, Sellmyer D J and Skomski R 2016 Structural disorder and magnetism in the spin-gapless semiconductor CoFeCrAl *AIP Adv.* **6** 056304
[13] Žic M *et al* 2016 Designing a fully compensated half-metallic ferrimagnet *Phys. Rev.* B **93** 140202
[14] Kharel P, Huh Y, Al-Aqtash N, Valloppilly S, Sabirianov R F, Skomski R and Sellmyer D J 2014 Structure and magnetic transitions in cubic Mn_3Ga *J. Phys.: Condens. Matter* **26** 126001
[15] Huh Y, Kharel P, Valloppilly S, Li X Z, Skomski R and Sellmyer D J 2013 Magnetism and electron transport of MnyGa ($1 < y < 2$) nanostructures *J. Appl. Phys.* **114** 013906
[16] Fujii S, Okada M, Ishida S and Asano S 2008 High spin polarizaion of ferrimagnetic Heusler-type alloys in Mn–Cr–Z system (Z = IIIb, IVb, Vb elements) *J. Phys. Soc. Japan* **77** 074702
[17] Luo H Z, Zhu Z Y, Liu G D, Xu S F, Wu G H, Liu H Y, Qu J P and Li Y X 2008 Prediction of half-metallic properties for the Heusler alloys Mn_2CrZ (Z = Al, Ga, Si, Ge, Sb): a first-principles study *J. Magn. Magn. Mater.* **320** 421
[18] Xing N S, Li H, Dong J M, Long R and Zhang C W 2008 First-principle prediction of half-metallic ferrimagnetism of the Heusler alloys Mn_2CoZ (Z = Al, Ga, Si, Ge) with a high-ordered structure *Comput. Mater. Sci.* **42** 600
[19] Sokolovskiy V V, Buchelnikov V D, Zagrebin M A, Entel P, Sahoo S and Ogura M 2012 First-principles investigation of chemical and structural disorder in magnetic Ni_2 Mn_{1+x} Sn_{1-x} Heusler alloys *Phys. Rev.* B **86** 134418
[20] Khmelevskyi S, Simon E and Szunyogh L 2015 Antiferromagnetism in Ru_2MnZ (Z = Sn, Sb, Ge, Si) full Heusler alloys: effects of magnetic frustration and chemical disorder *Phys. Rev.* B **91** 094432
[21] Zhang W Y, Kharel P, Skomski R, Valloppilly S, Li X Z and Sellmyer D J 2016 Structure, magnetism, and electron-transport properties of Mn_2CrGa-based nanomaterials *AIP Adv.* **6** 056218
[22] Jin Y *et al* 2016 Half-metallicity in highly $L2_1$-ordered CoFeCrAl thin films *Appl. Phys. Lett.* **109** 142410
[23] Kobayashi K, Umetsu R Y, Kainuma R, Ishida K, Oyamada T, Fujita A and Fukamichi K 2004 Phase separation and magnetic properties of half-metal-type $Co_2Cr_{1-x}Fe_x$ Al alloys *Appl. Phys. Lett.* **85** 4684
[24] Karthik S V, Rajanikanth A, Takahashi Y K, Okhubo T and Hono K 2006 Spin polarization of quaternary $Co_2Cr_{1-x}Fe_xAl$ Heusler alloys *Appl. Phys. Lett.* **89** 052505
[25] Miura Y, Nagao K and Shirai M 2004 Atomic disorder effects on half-metallicity of the full-Heusler alloys $Co_2(Cr_{1-x}Fe_x)$ Al: a first-principles study *Phys. Rev.* B **69** 144413
[26] Nayak A K *et al* 2015 Design of compensated ferrimagnetic Heusler alloys for giant tunable exchange bias *Nat. Mater.* **14** 679
[27] Galanakis I and Şaşıoğlu E 2011 High T_C half-metallic fully-compensated ferrimagnetic Heusler compounds *Appl. Phys. Lett.* **99** 052509
[28] Wurmehl S, Kandpal H C, Fecher G H and Felser C 2006 Valence electron rules for prediction of halfmetallic compensated-ferrimagnetic behaviour of Heusler compounds with complete spin polarization *J. Phys.: Condens. Matter* **18** 6171
[29] van Leuken H and de Groot R A 1995 Half-metallic antiferromagnets *Phys. Rev. Lett.* **74** 1171
[30] Rode K *et al* 2013 Site-specific order and magnetism in tetragonal Mn_3Ga thin films *Phys. Rev.* B **87** 184429
[31] Betto D, Lau Y C, Borisov K, Kummer K, Brookes N B, Stamenov P, Coey J M D and Rode K 2017 Structure, site-specific magnetism, and magnetotransport properties of epitaxial $D0_{22}$-structure Mn_2Fe_xGa thin films *Phys. Rev.* B **96** 024408
[32] Gasi T, Nayak A K, Winterlik J, Ksenofontov V, Adler P, Nicklas M and Felser C 2013 Exchange-spring like magnetic behavior of the tetragonal Heusler compound Mn_2FeGa as candidate for spin-transfer torque *Appl. Phys. Lett.* **102** 202402
[33] Liu Z H, Zhang Y J, Zhang H G, Zhang X J and Ma X Q 2016 Giant exchange bias in Mn_2FeGa with hexagonal structure *Appl. Phys. Lett.* **109** 032408
[34] Nayak A K, Nicklas M, Chado S, Shekhar C, Skourski Y, Winterlik J and Felser C 2013 Large zero-field cooled exchange-bias in bulk Mn_2PtGa *Phys. Rev. Lett.* **110** 127204
[35] Galanakis I and Dederichs P H and Papanikolaou N 2002 Slater–Pauling behavior and origin of the half-metallicity of the full-Heusler alloys *Phys. Rev.* B **66** 174429
[36] Mizukami S, Sugihara A, Iihama S, Sasaki Y, Suzuki K Z and Miyazaki T 2016 Laser-induced THz magnetization precession for a tetragonal Heusler-like nearly compensated ferrimagnet *Appl. Phys. Lett.* **108** 012404
[37] Jamer M E *et al* 2017 Compensated ferrimagnetism in the zero-moment Heusler alloy Mn_3Al *Phys. Rev. Appl.* **7** 064036
[38] Kurt H, Rode K, Stamenov P, Venkatesan M, Lau Y C, Fonda E and Coey J M D 2014 Cubic Mn_2Ga thin films:

crossing the spin gap with ruthenium *Phys. Rev. Lett.* **112** 027201
[39] Deka B, Singh R K and Srinivasan A 2015 Search for fully compensated ferrimagnet in Co substituted Mn_2VGa alloy *J. Magn. Magn. Mater.* **395** 240
[40] Feng W W, Fu X, Wan C H, Yuan Z H, Han X F, Quang N V and Cho S 2015 Spin gapless semiconductor like Ti_2MnAl film as a new candidate for spintronics application *Phys. Status Solidi RRL* **9** 641
[41] Soulen R J *et al* 1998 Measuring the spin polarization of a metal with a superconducting point contact *Science* **282** 85
[42] Upadhyay S K, Palanisami A, Louie R N and Buhrman R A 1998 Probing ferromagnets with Andreev reflection *Phys. Rev. Lett.* **81** 3247
[43] Bainsla L, Yilgin R, Okabayashi J, Ono A, Suzuki K and Mizukami S 2017 Structural and magnetic properties of epitaxial thin films of the equiatomic quaternary CoFeMnSi Heusler alloy *Phys. Rev.* B **96** 094404
[44] Smart J S 1966 *Effective-Field Theories of Magnetism* (Philadelphia, PA: Saunders)
[45] Skomski R 2008 *Simple Models of Magnetism* (Oxford: Oxford University Press)
[46] Nayak A K, Nicklas M, Shekhar C and Felser C 2013 Kinetic arrest related to a first-order ferrimagnetic to antiferromagnetic transition in the Heusler compound Mn_2PtGa *J. Appl. Phys.* **113** 17E308
[47] Nayak A K, Sahoo R, Salazar Mejia C, Nicklas M and Felser C 2015 Magnetic phase coexistence and metastability caused by the first-order magnetic phase transition in the Heusler compound Mn_2PtGa *J. Appl. Phys.* **117** 17D715
[48] Stinshoff R, Nayak A K, Fecher G H, Balke B, Ouardi S, Skourski Y, Nakamura T and Felser C 2011 Completely compensated ferrimagnetism and sublattice spin crossing in the half-metallic Heusler compound $Mn_{1.5}FeV_{0.5}Al$ *Phys. Rev.* B **95** 060410
[49] Mooij J H 1973 Electrical conduction in concentrated disordered transition metal alloys *Phys. Status Solidi* a **17** 521
[50] Allen P B 2006 Electron transport *Conceptual Foundations of Materials: a Standard Model for Ground- and Excited-State Properties* ed S G Louie and M L Cohen (Amsterdam: Elsevier) ch 6 pp 165–218
[51] Jin Y, Skomski R, Kharel P, Valloppilly S R and Sellmyer D J 2017 Effect of disorder on the resistivity of CoFeCrAl films *AIP Adv.* **7** 055834
[52] Mazin I I 1999 How to define and calculate the degree of spin polarization in ferromagnets *Phys. Rev. Lett.* **83** 1427
[53] Kharel P, Thapa P, Lukashev P, Sabirianov R F, Tsymbal E Y, Sellmyer D J and Nadgorny B 2011 Transport spin polarization of high Curie temperature MnBi films *Phys. Rev.* B **83** 024415
[54] Chen T Y, Huang S X and Chien C L 2010 Pronounced effects of additional resistance in Andreev reflection spectroscopy *Phys. Rev.* B **81** 214444
[55] Rajanikanth A, Takahashi Y K and Hono K 2007 Spin polarization of Co_2MnGe and Co_2MnSi thin films with A2 and $L2_1$ structures *J. Appl. Phys.* **101** 023901
[56] Bainsla L, Suresh K G, Nigam A K, Manivel Raja M, Varaprasad B S D C S, Takahashi Y K and Hono K 2014 High spin polarization in CoFeMnGe equiatomic quaternary Heusler alloy *J. Appl. Phys.* **116** 203902
[57] Kharel P, Zhang W, Skomski R, Valloppilly S, Huh Y, Fuglsby R, Gilbert S and Sellmyer D J 2015 Magnetism, electron transport and effect of disorder in CoFeCrAl *J. Phys. D: Appl. Phys.* **48** 245002